ACI STRUCTURAL JOURNAL TECHNICAL PAPER

Title No. 122-S48

Modified Analytical Model for Shear Capacity of Corroded Columns

by Benjamin Matthews, Alessandro Palermo, and Allan Scott

This paper proposes a series of empirical modifications to an existing three-step analytical model used to derive the cyclic shear capacity of circular reinforced concrete (RC) columns considering corrosive conditions. The results of 16 shear-critical RC columns, artificially corroded to various degrees and tested under quasi-static reversed cyclic loading, are used for model verification. The final model is proposed in a piecewise damage-state format relative to the measured damage of the steel reinforcement. New empirical decay coefficients are derived to determine the degraded material properties based on an extensive database of over 1380 corroded tensile tests. An additional database of 44 corroded RC circular piers is collected to assist in the modification of ductility-based parameters. Compared to the shear-critical test specimens, the model results indicate that the peak shear capacity can be predicted well across a range of deterioration severities (0 to 58.5% average transverse mass loss), with a mean predictive ratio of ±8.60%. As damage increases, the distribution of the corrosion relative to the location of the shear plane becomes a critical performance consideration, increasing predictive variance.

Keywords: analytical model; circular columns; corrosion; cyclic; reinforced concrete (RC); shear.

INTRODUCTION

Aging reinforced concrete (RC) infrastructure is at risk of continual degradation throughout its service life due to aggressive environmental factors and construction/design deficiencies.[1,2] Chlorides permeating the protective concrete cover eventually depassivate the embedded steel reinforcement, generating expansive rust products.[3] As the steel oxidizes locally, internal radial stresses are introduced. Once expansive pressures exceed the pore pressure and concrete tensile splitting capacity, microcracking proliferates throughout the porous material. The presence of microcracks accelerates the diffusion of chloride ions and oxygen from the concrete surface toward the steel interface.[1,4] As corrosion advances, cracking develops into visible macrocracks, which detrimentally affect the mechanical response of the material through a redistribution of the constitutive stress-strain pathways.[1] At severe degradation, cracks develop into the confined concrete core, compromising the structural reliability of the member to withstand seismic loads.[5]

Transverse reinforcement possesses the most significant risk of chloride-induced deterioration due to the conventional geometric and physical design of RC members. The transverse steel is typically detailed as the outer-facing reinforcement, which leads to a smaller thickness of concrete cover protection from chloride ingress.[6,7] Compared to the larger longitudinal bars, the smaller transverse diameter also oxidizes proportionately faster. Thus, transverse steel is often observed to deteriorate preferentially, with ratios of transverse-longitudinal corrosion ranging between 1.5 and 4.5.[8,9] An accelerated loss of transverse steel will lead to a disproportionate degradation of shear and confinement-related mechanical properties. Understanding the disproportionate reduction of mechanical properties is crucial in structural reliability assessments of aging RC bridge structures, particularly those lacking adequate seismic resistance. Many aging bridge assets were designed to obsolete seismic guidelines, providing inadequate seismic design before the additional effects of long-term corrosion are even considered.[10,11] Thus, the degradation of the seismic shear capacity of RC columns is a critical concern to be addressed across the aging infrastructure stock.

LITERATURE REVIEW

The ability of an RC column to resist shear stresses imposed on the system by seismic loading is provided by the constitutive relationships between the concrete and steel materials. The concrete shear resistance is provided by the transfer of stress along the crack interface through the interlocking of aggregate protruding from the crack.[12] Transverse steel reinforcement intercepting the crack will mobilize and redistribute the tensile strain throughout the confining cage. Dowel action transfers stress from orthogonal cracks to the longitudinal reinforcement, increasing shear stiffness.[12] Axial compression amplifies the shear resistance of a column by increasing the effectiveness of aggregate interlock. Ang[13] and Priestley et al.[14] experimentally verified the direct correlation between axial load ratio and nominal shear capacity. ACI 318-19[15] provisions consider the contribution of the axial load to the shear resistance as an integral component of the concrete shear resistance. Other models, such as the Kowalsky and Priestley[16] model, developed at the University of California, San Diego (termed the UCSD model herein), disassociate axial and concrete contributions into individual terms. The concrete shear resistance is known to degrade in RC columns under substantial deflection due to the progressive loss of aggregate interlock transfer after excessive crack dilation and smoothening along the crack interface from continual abrasion.[17-19] Figure 1(a)

ACI Structural Journal, V. 122, No. 4, July 2025.

MS No. S-2023-212.R7, doi: 10.14359/51745466, received September 6, 2024, and reviewed under Institute publication policies. Copyright © 2025, American Concrete Institute. All rights reserved, including the making of copies unless permission is obtained from the copyright proprietors. Pertinent discussion including author's closure, if any, will be published ten months from this journal's date if the discussion is received within four months of the paper's print publication.

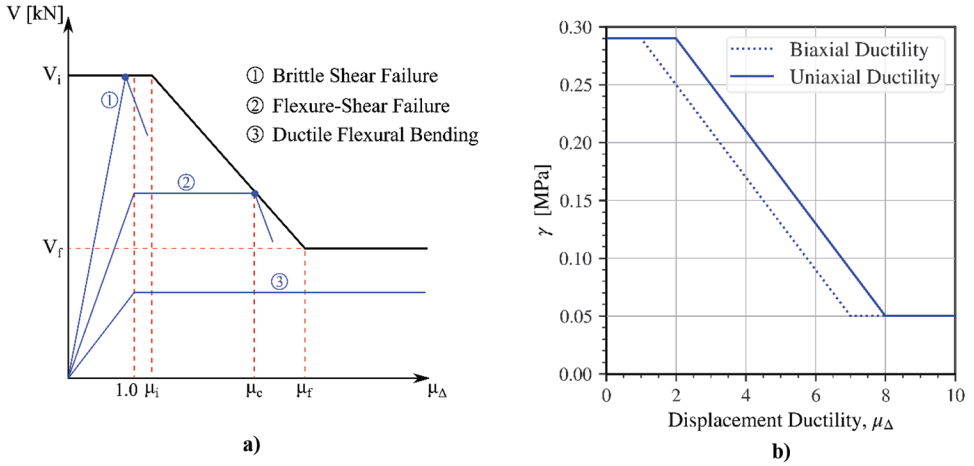

Fig. 1—(a) Joint ASCE-ACI Task Committee 426[17] shear-ductility model[18]; and (b) UCSD γ model for degradation of concrete shear resistance with increasing displacement ductility.[16]

illustrates the original conceptual model for shear capacity in RC column sections, proposed by Joint ASCE-ACI Task Committee 426[17] and adapted by Ang et al.[18]

Ang et al.[18] and Wong et al.[19] derived relationships between the degradation in concrete shear resistance and the increase in displacement ductility. Priestley et al.[14] then proposed a displacement ductility factor, γ, by integrating the Ang and Wong ductility models to account for degradation in concrete contribution at high displacement ductility. Figure 1(b) presents the γ-curve for the displacement ductility modified by Kowalsky and Priestley[16] for RC columns with circular cross sections. Other models proposed ductility-related factors to a similar effect, including Aschheim and Moehle[20] (UCB model), the California Department of Transportation[21] (Caltrans model), and Applied Technology Council[22] (ATC model). For circular cross sections, seismic design codes such as ACI 318-19 suggest indirectly deriving an equivalent square or rectangular section to calculate the nominal shear capacity. NZS 3101.1&2:2006[23] directly evaluates the nominal shear capacity using the actual circular section, replacing the total gross cross section with an effective shear area component. Cai et al.[24] evaluated the previously mentioned models and proposed a new approach, correlating the seismic shear capacity with the column drift ratio, to alleviate the ambiguity around ductility-based design. The proposed model effectively calculated the seismic shear capacity of circular columns without requiring transformation into an equivalent square or rectangular section.

Under ordinary uncorroded conditions, the aforementioned models provide reliable estimations of the cyclic shear capacity of RC columns with various cross sections. However, when considering the debilitating effects of chloride-induced corrosion, the mechanical reliability of the degraded materials is compromised and must be reevaluated. An abundance of experimental research has been conducted on corroded RC columns with square and rectangular sections.[7,25-29] A much smaller volume of experimental data exists on corroded circular sections.[6,8,30-32] An experimental program conducted by the authors investigated the rate of seismic shear loss in short shear-critical RC circular columns under various levels of imposed corrosion damage.[33] Test observations indicated that deflection capacity was much more heavily impacted by corrosion than the peak shear capacity. A maximum reduction of 70.9% and 37.5% was recorded for the ultimate displacement and peak shear capacity, respectively, at average mass losses of 8.87% and 37.7% for the longitudinal and transverse reinforcement. Li et al.[32] proposed an empirical relationship between the average transverse mass loss, axial load ratio, and residual shear capacity based on the results of four corroded short circular piers failing in shear. Li et al.[33] extended this analysis by proposing a constitutive model based on the Modified Compression Field Theory and a nonlinear finite element analysis. Using additional experimental results of square columns failing in shear, the proposed model appeared to predict the residual shear capacity well, with prediction ratios ranging between 0.78 and 1.26.

This paper proposes a series of modifications to the revised UCSD model used to calculate the seismic shear capacity of RC circular columns under corrosive conditions. The UCSD model presented by Kowalsky and Priestley[16] is selected as the basis of this investigation as a highly effective model with a direct evaluation of the circular section. The changes integrate the effects of material and mechanical degradation of members exposed to chloride-induced corrosion on the peak shear capacity. To the best of the authors' knowledge, the experimental tests reported in this study and Li et al.[32] are the only programs that involve the corroded behavior of RC circular columns failing in shear-dominated modes. Due to several essential cracking statistics not reported in Li et al.,[32] the proposed modifications are developed primarily around the experiments presented by Matthews et al.[34] A database of 44 corroded circular columns, failing under various modes and ductilities, is compiled to derive new relationships between concrete shear degradation and displacement ductility.

RESEARCH SIGNIFICANCE

The implications of material and mechanical degradation on the structural performance of chloride-affected columns must be known to estimate the remaining capacity of aging structures. Shear failure of short shear-critical columns is a

Table 1—Column specimen geometric, reinforcement, and corrosion design parameters

Column ID	f_c', MPa	ρ_{sp}, %	s, mm	d_{sp}, mm	L, mm	i_{corr}, μA/cm^2	t, days	$\eta_{m,l}$, %	$\eta_{m,sp}$, %
BM-UC	37.4	0.57	125	10	1075	0	0	0	0
UC-L1	47.1	0.57	125	10	1075	200	20	4.87	13.20
UC-L2-2.95	47.1	0.57	125	10	1475	300	13	4.56	12.32
UC-M1	46.7	0.57	125	10	1075	200	69	7.88	37.49
UC-M2	47.1	0.57	180	12	1075	200	69	8.97	27.16
UC-S1	46.7	057	125	10	1075	200	123	10.51	42.96
UC-S2-2.95	47.1	0.57	125	10	1475	300	80	9.45	30.44
BM-WC	35.9	1.10	65	10	1075	0	0	0	0
CS-L1	56.7	1.10	65	10	1075	200	20	4.96	16.30
CS-L2	46.7	1.10	65	10	1075	300	13	5.10	15.22
CS-S1	56.7	1.10	65	10	1075	200	123	13.21	58.51
CS-S2	56.7	1.10	65	10	1075	300	82	12.83	52.43
WD-WC-L1	56.7	1.10	65	10	1075	200	20	4.38	12.16
WD-WC-L2	38.6	1.10	65	10	1075	300	13	4.40	15.48
WD-WC-M1	56.7	1.10	65	10	1075	200	69	5.81	28.68
WD-WC-M2	47.1	1.10	95	12	1075	200	69	7.68	27.70
WD-WC-S1	56.7	1.10	65	10	1075	200	123	8.87	37.69
WD-WC-S2	46.7	1.10	65	10	1075	300	82	7.61	35.70

Note: CS is constant saturation; WD is wetting-and-drying cycles; BM is benchmark uncorroded; UC is under-confined; WC is well-confined; L is low target corrosion; M is moderate corrosion; S is severe target corrosion; and the suffix 2.95 refers to the change in aspect ratio.

crucial design and safety consideration due to its brittle and often explosive nature. Because transverse reinforcement typically suffers from more severe degradation than longitudinal reinforcement, ductile members designed with low flexural-to-shear capacity ratios are also at substantial risk of triggering brittle shear-dominated failure modes. This paper proposes a series of modifications to an existing analytical approach to predict the cyclic shear capacity of corroded RC circular columns. A piecewise damage-state format for low, moderate, and severe corrosion damage is suggested. The effects of corrosion on material and mechanical properties are investigated separately, with two new coefficients proposed to account for: 1) premature loss of bond due to severe degradation; and 2) an initial enhancement in shear stress transfer due to existing corrosion surface cracks. The proposed model provides an enhanced predictive ability for moderately to highly corroded RC columns with longitudinal mass losses greater than 7.5%.

EXPERIMENTAL DATA

An experimental study was undertaken at the University of Canterbury in New Zealand to investigate the cyclic shear performance of 16 artificially corroded RC short circular piers. All piers were designed to trigger shear-dominated failure modes. Tests were performed under displacement-controlled quasi-static fully reversed cyclic loading using a standard cyclic loading protocol.[35] The study variables included corrosion current density, corrosion damage level, confinement effectiveness, spiral diameter size effect, and aspect ratio (L/D).

All columns were designed with a 500 mm diameter (D) and a cover thickness of 25 mm. Two transverse volumetric ratios were implemented to categorize different levels of confinement effectiveness: under-confined (UC) and well-confined (WC).[23] A low axial compression ratio of 0.02 was used to minimize the shear-resistance mechanisms enhanced by axial force.[16] Two variations of the impressed-current accelerated corrosion method were implemented: cyclic wetting and drying (WD) and constant saturation (CS). A wet-to-dry ratio of 4:3 was adopted for the entire corrosion incubation. All UC columns were subjected to cyclic wetting-and-drying periods. A 200 or 300 μA/cm^2 current density was applied to each specimen.

Table 1 summarizes the key design and corrosion parameters for each column in this study, where f_c' is the concrete compressive strength at testing; ρ_{sp} is the transverse volumetric ratio; s is the spiral spacing; d_{sp} is the nominal spiral diameter; i_{corr} is the applied current density; t is the duration of the corrosion exposure; and $\eta_{m,l}$ and $\eta_{m,sp}$ are the average longitudinal and spiral mass loss percentages, respectively. For brevity, the experimental design details, test setup, and structural analyses are not discussed in this paper; they can be found in Matthews et al.[34] Figure 2(a) presents the standard design used for the benchmark specimens, and Fig. 2(b) illustrates the cyclic test setup used in this program. Table 2 summarizes the structural test results for each specimen, where θ is the inclination angle of the primary diagonal strut to the column axis; Δ_u is the ultimate displacement measured at 0.85 of the peak load; and μ_Δ is the displacement ductility.

Table 2—Structural results from cyclic testing

Specimen ID	P, kN	θ, deg	Δ_y, mm	V_y, kN	V_{max}^+, kN	V_{max}^-, kN	Δ_u, mm	μ_Δ	Failure mechanism
BM-UC	147	27.8	7.57	433	500	444	32.1	4.24	Shear limited ductility
UC-L1	185	24.0	8.13	422	483	513	19.2	2.36	Shear limited ductility
UC-L2-2.95	185	25.8	24.81	465	498	424	35.6	1.44	Brittle shear
UC-M1	183	24.0	11.53	509	588	535	15.2	1.32	Brittle shear
UC-M2	185	24.4	7.66	422	478	408	12.1	1.59	Brittle shear-bond
UC-S1	183	23.7	8.63	414	474	495	15.2	1.77	Brittle shear
UC-S2-2.95	185	22.1	16.01	339	391	345	23.3	1.45	Brittle shear-bond
BM-WC	141	38.1	13.00	639	689	640	36.2	2.78	Shear limited ductility
CS-L1	223	25.0	14.81	621	671	638	23.2	1.57	Brittle shear
CS-L2	183	26.4	13.37	610	670	680	27.8	2.08	Shear limited ductility
CS-S1	223	0.0	9.28	424	518	491	15.4	1.65	Brittle shear-bond
CS-S2	223	0.0	13.00	476	507	501	19.7	1.52	Brittle shear-bond
WD-WC-L1	223	30.9	14.40	652	725	764	30.8	2.14	Shear limited ductility
WD-WC-L2	152	28.6	13.51	537	637	592	28.2	2.09	Shear limited ductility
WD-WC-M1	223	25.9	11.35	577	671	632	19.2	1.69	Brittle shear
WD-WC-M2	185	25.2	15.87	612	706	645	27.1	1.71	Brittle shear
WD-WC-S1	223	20.3	7.16	370	420	430	10.5	1.47	Brittle shear-bond
WD-WC-S2	183	30.1	9.97	427	493	444	16.0	1.61	Brittle shear-bond

Note: V_{max}^+ represents maximum shear force experienced in push direction; V_{max}^- represents maximum shear force experienced in pull direction.

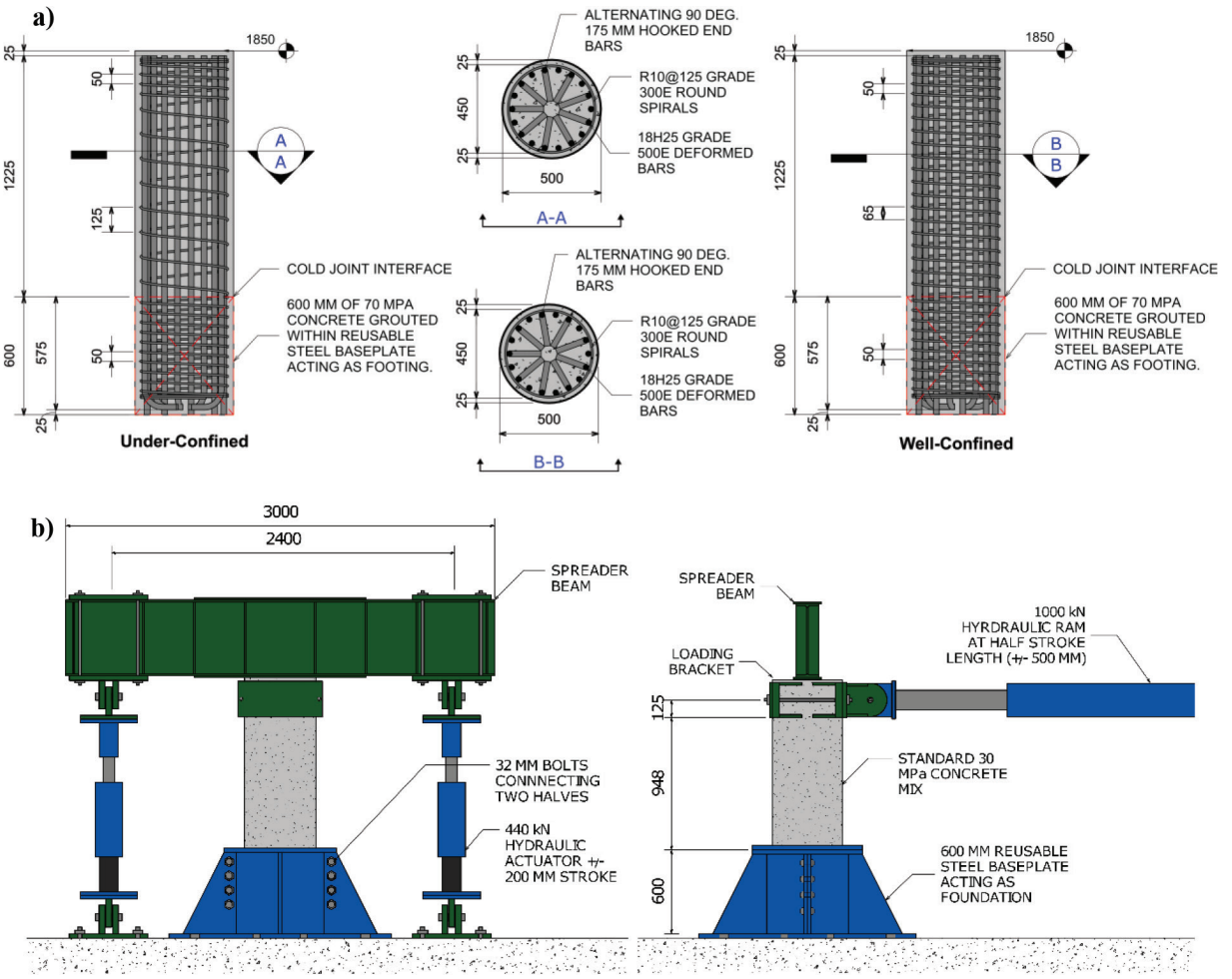

Fig. 2—(a) Standard under-confined and well-confined column designs; and (b) cyclic shear test setup.

SHEAR MODELS

A comparative analysis of several analytical models with ascending complexity is presented to verify the efficacy of the final proposed model. The Kowalsky and Priestley[16] revised UCSD model for uncorroded columns is included to serve as a predictive benchmark (*M*-0). Two additional simplified degradation models are selected. The first derives a simple shear capacity reduction factor relative to the average longitudinal mass loss (*M*-1). The second considers only the degraded material properties of the steel reinforcement (*M*-2). Finally, based on the revised UCSD model structure, the complete degradation model is proposed in a piecewise format relative to different corrosion damage limit states (*M*-3).

Revised UCSD shear model *M*-0

Kowalsky and Priestley[16] presented revisions to the analytical model for the cyclic shear capacity of circular RC columns originally proposed by Priestley et al.,[14] based on the work performed by Ang et al.[18] and Wong et al.[19] This study proposes modifications to the Kowalsky and Priestley[16] revision, which may serve as a useful analytical tool for the simplified estimation of the degraded shear capacity of corroded circular columns. The UCSD-A model (assessment model) defines the nominal shear capacity of a circular column in the form

$$V_A = V_s + V_p + V_c \tag{1}$$

$$V_s = \frac{\pi}{2} A_{sp} f_{yt} \frac{D - c - \delta}{s} \cot(\theta) \tag{2}$$

$$V_p = P \frac{(D - c)}{2L} \text{ for } P > 0 \tag{3}$$

$$V_c = \alpha \beta \gamma \sqrt{f_c'} (0.8 A_g) \tag{4}$$

The model is characterized by the shear resistance provided by the steel truss mechanism (V_s), the axial load component (V_p), and the concrete mechanism (V_c), where f_{yt} is the nominal yield capacity of the transverse reinforcement; c is the neutral axis depth; δ represents the depth of the cover concrete to the transverse reinforcement layer; the strut inclination angle θ is assumed to be 30 degrees; α is a factor accounting for column aspect ratio; β accounts for the longitudinal steel ratio; γ represents the reduction in concrete shear resistance with increasing ductility; and A_g is the gross cross-sectional area of the column. The original uncorroded shear model is designated herein as model *M*-0. Due to insufficient experimental data on corroded columns failing in shear with adequate ranges of aspect ratios and longitudinal steel ratios, modifications to α and β are considered outside of the scope of this research. Equations (5) and (6) present the original α and β curves proposed by Kowalsky and Priestley[16]

$$1 \le \alpha = 3 - (M/VD) \le 1.5 \tag{5}$$

$$\beta = 0.5 + 20\rho_l \le 1.0 \tag{6}$$

where M/VD is equivalent to L/D; and ρ_l is the longitudinal reinforcement ratio.

Simple degradation model *M*-1

Model *M*-1 includes a simple empirical degradation factor, defined by the loss of shear capacity with increasing average longitudinal mass loss ($\eta_{m,l}$) relative to the uncorroded benchmark, expressed by Eq. (7). The maximum shear capacity is normalized against the dependable section, $A_g\sqrt{f_c'}$, to eliminate the influence of different concrete compressive strengths. The degradation coefficient is derived statistically through an ordinary least squares (OLS) evaluation, resulting in the linear relationship described in Eq. (7)

$$V_{max,corr} = (1 - 0.0377\eta_{m,l}) V_{max,0} \tag{7}$$

where $V_{max,0}$ is derived theoretically from Eq. (1) (that is, model *M*-0). $V_{max,0}$ is equal to 470.0 and 618.7 kN for BM-UC and BM-WC, respectively. The Eq. (7) prediction provides an R^2 of 0.520 and a mean absolute percentage error (MAPE) of 9.80%.

Simple degradation model *M*-2

The second degradation model (*M*-2) adopts the UCSD model, substituting the material properties for their degraded estimates. The mean residual cross-sectional area of the transverse reinforcement and the residual spiral yield capacity are considered here, given in Eq. (8) to (11).

Area loss—As the reinforcing steel deteriorates with time, the geometric properties degrade at a proportional rate. The average residual cross-sectional area of the degrading steel is equivalent to the average mass loss measured gravimetrically, shown as

$$\frac{m_0 - m_{corr}}{m_0} = \frac{A_0 - A_{corr}}{A_0} = \frac{Ø_0^2 - Ø_{corr}^2}{Ø_0^2}$$

Thus, the mean residual bar diameter and cross-sectional area of the steel reinforcement can be inferred from the average mass loss percentage as

$$Ø_{res} = Ø_0 - Ø_0\left(1 - \sqrt{1 - \eta_m}\right) \tag{8}$$

$$A_{res} = A_0(1 - \eta_m) \tag{9}$$

Reinforcement yield capacity—Strength-based mechanical properties have been shown throughout the literature to degrade linearly with increasing average mass loss. Imperatore[36] conducted a detailed review of existing empirical formulations for estimating several key mechanical properties of steel. Empirical coefficients for the yield stress of a corroded bar have been found to range from 0.0016 to 0.0198 for artificially corroded bars and from 0.0119 to 0.0143 for naturally corroded bars.[37-43] The degraded yield stress presented herein is considered relative to the nominal uncorroded area of the bar (engineering stress) rather than a function of the residual area.

This study uses a database of over 1380 monotonic tensile tests on corroded reinforcing bars to update the empirical coefficient for the yield stress of the transverse reinforcement. The open-source database compiled by the authors for a previous study can be found at https://zenodo.org/records/8035720. Separating the data by corrosion type results in two data sets of 674 artificially corroded samples and 530 naturally corroded samples. Because morphological properties vary widely in large-scale structural members, this study only considers a coefficient of variation in the corrosion method. Equation (10) presents the relationship between the normalized yield stress and average mass loss for different corrosion types.

$$f_{y,res} = \alpha_y f_{y0} \tag{10}$$

$$f_{y,res} = \begin{cases} (1.0 - 0.0183\eta_m)f_{y0},\ 0 < \eta_m < 27.5\%\ \text{(Artificial)} \\ (1.0 - 0.0101\eta_m)f_{y0},\ 0 < \eta_m < 27.5\%\ \text{(Natural)} \\ (0.82 - 0.0086\eta_m)f_{y0},\ \eta_m \geq 27.5\%\ \text{(Combined)} \end{cases}$$

A change in the degradation slope was observed at larger mass loss magnitudes, indicating a bilinear degradation trend. For severe column damage states, specimens demonstrated transverse mass losses typically between 27.7 and 58.5%. Therefore, the degradation slope was defined into bilinear ranges of $0\% < \eta_m < 27.5\%$ and $27.5\% < \eta_m < 100\%$, and the corresponding yield coefficient, α_y, was statistically derived using an OLS evaluation. Due to the scarce available data in the higher degradation range, natural and artificial samples were combined to improve the model fit. The coefficient of determination, R^2, was calculated as 0.98, 0.984, and 0.921 for earlier artificial and natural ranges and the severe combined range, respectively. Because the degraded engineering stress derived in Eq. (10) is measured relative to the nominal uncorroded cross-sectional area, the appropriate modification to Eq. (2) becomes

$$V_s = \frac{\pi}{2}\alpha_y(A_{sp,0}f_{yt,0})\frac{D - c - \delta}{s}\cot(\theta) \tag{11}$$

M-3 PROPOSED MODIFICATIONS

Model structure

The proposed modifications to the UCSD model follow a damage-dependent structure as a function of the average mass loss of the longitudinal steel. Longitudinal mass loss is selected as the governing criterion due to more consistent experimental reliability than transverse mass loss (Table 1). From the available data, four key damage states can be identified.

Damage state 0 (DS0)—DS0 is uncorroded. The model remains unchanged from Eq. (1) to (4).

Damage state 1 (DS1)—DS1 can be identified by low corrosion, pre-cracking. Bond strength is observed to increase slightly due to the additional friction the rust provides[44,45] before expansive pressures exceed the tensile strength of the concrete cover. Oh et al.[46] proposed a critical mass loss ($\eta_{m,crit}$) threshold for the initiation of concrete cover cracking relative to the cover depth

$$\eta_{m,crit} = 0.0018\delta^{2.07} \tag{12}$$

For a cover depth (δ) of 25 mm, the critical mass loss threshold is approximately 1.4%. Ou et al.[47] and Cheng et al.[48] adopted a value of 1.5% for an equivalent uncorroded condition. Thus, until reaching $\eta_{m,crit}$, Eq. (1) to (4) are maintained. DS1 is defined over the range

$$0 < \eta_{m,l,\text{DS1}} \leq \eta_{m,crit} \tag{13}$$

Damage state 2 (DS2)—DS2 has moderate corrosion and an initial post-cracking stage with early reductions in concrete and steel material properties. It is characterized by changes to the material properties and mechanical structure of the shear mechanisms while still maintaining a ductile failure mode. $\eta_{m,l} = 7.5\%$ corresponds approximately to the threshold between ductile and brittle shear failures (Tables 1 and 2). Beyond this, the transverse mass loss exceeds 27.5%. DS2 is therefore defined as

$$\eta_{m,crit} < \eta_{m,l,\text{DS2}} \leq 7.5\% \tag{14}$$

Damage state 3 (DS3)—DS3 has severe corrosion, significant longitudinal and transverse cracking, concrete decay (powdering), cover spalling, and expected cracking into the concrete core. Due to the lattice-like interwoven crack pattern, the cover is treated as a delaminated body from the rest of the rigid member and is assumed to be largely ineffective at carrying stress. Brittle failures are characteristic of this damage state. It is common to observe localized hotspots of 100% spiral reduction, causing confinement to become effectively reliant on the contribution of the longitudinal bars over a given region. DS3 is defined by corrosion damage exceeding 7.5% mass loss of the longitudinal steel, with an average transverse mass loss greater than 27.5%.

$$\eta_{m,l,\text{DS3}} > 7.5\% \tag{15}$$

Material modifications

Steel elastic modulus—The degradation in steel elastic modulus, measured relative to the engineering yield stress, can be derived using the same aforementioned database through Eq. (16). After separating by corrosion type, 575 artificially corroded and 195 naturally corroded samples were available for analysis.

$$E_{s,res} = \begin{cases} (1.0 - 0.0105\eta_m)E_{s0} & \text{if Artificial} \\ (1.0 - 0.0127\eta_m)E_{s0} & \text{if Natural} \end{cases} \tag{16}$$

where E_{s0} is the uncorroded steel elastic modulus, assumed to be 200 GPa. The linear regression in Eq. (16) produced an R^2 of 0.646 and 0.892 for artificial and natural predictions, respectively.

Concrete compressive strength—Corrosion cracking affects the member on both material and mechanical levels. Campione et al.[5] proposed a corroded section model for circular columns considering three critical zones: 1) the cracked concrete cover; 2) a cracked portion of the concrete core; and 3) the uncracked concrete core. Figure 3 illustrates

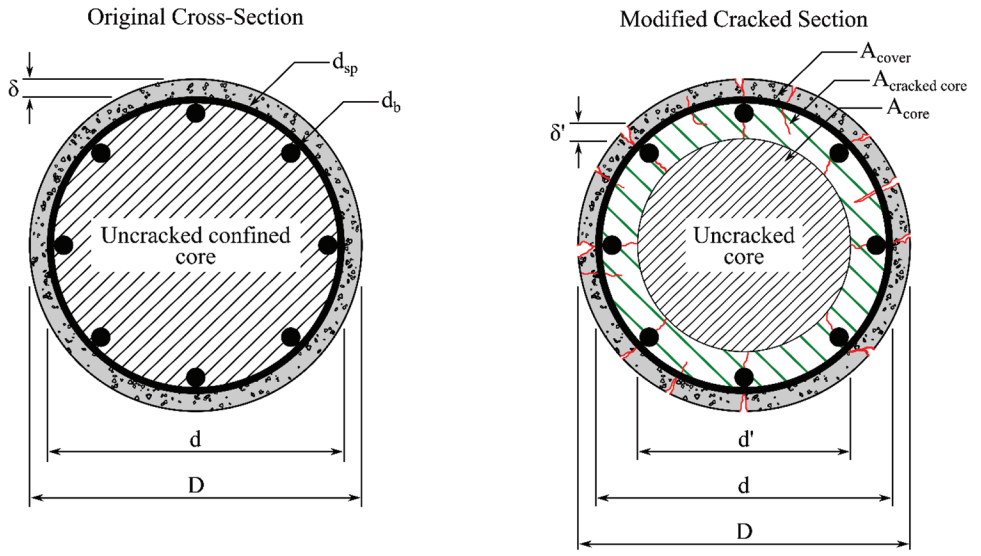

Fig. 3—Corroded section model for material modifications.

the section model adopted for this analysis. The model assumes that rust products accumulate uniformly around the bar circumference, are incompressible, and thus generate expansive microcracks bilaterally.[49] The cracked portion of the core is estimated to have a uniform depth equal to the cover concrete, $\delta' \approx \delta$.

Cracked concrete cover—Corrosion-induced cracking proliferating throughout the concrete cover will alter the constitutive stress-strain relationships between the steel, concrete, and applied loads. For unconfined concrete, the softening coefficient, ζ_{uc}, is described as[50]

$$f_{c,corr}' = \zeta_{uc} f_c' \tag{17}$$

$$\zeta_{uc} = \begin{cases} 1.0 & \varepsilon_{cr} = 0 \\ \dfrac{0.9}{\sqrt{1 + 600\varepsilon_{cr}}} & \varepsilon_{cr} \geq 0 \end{cases} \tag{18}$$

$$\varepsilon_{cr} = \frac{w_{cr,tot}}{b_0} \tag{19}$$

$$w_{cr,tot} = \frac{\sum w_{cr,i} l_i}{L} \tag{20}$$

where $f_{c,corr}'$ is the corroded unconfined concrete strength; ε_{cr} is the tensile strain induced by the corrosion cracking; b_0 is the column circumference; $w_{cr,tot}$ is the total surface crack width measured experimentally; $w_{cr,i}$ is the crack width increment, assumed to be approximately constant over the measured length l_i; and L is the column clear height.[51] This method geometrically accounts for any subjectiveness in classifying constant crack width between experiments.

Cracked concrete core—The compressive strength of the cracked zone of the confined core, f_{ccc}, can be estimated using a theoretical prediction of the softening coefficient. The degraded confinement effectiveness will adversely affect the confined concrete strength[52]

$$f_{ccc} = \zeta_{cc} f_c' \left(-1.254 + 2.254\sqrt{1 + \frac{7.94K}{f_c'}} - 2\frac{K}{f_c'} \right)$$

$$f_{ccc} = \zeta_{cc} f_c' \cdot \alpha_K \tag{21}$$

where α_K is the simplified confinement magnifier. Using Eq. (18) and (19), ζ_{cc} can be determined by substituting a theoretical estimation of the total crack width within this zone[53]

$$w_{cr,th} = 2\pi(v_{rs} - 1)P_{ave} \tag{22}$$

where v_{rs} is the volumetric expansion ratio between the corrosion product and base metal, taken equal to 2;[53] and P_{ave} is the average penetration based on uniform corrosion, determined either experimentally or estimated theoretically[54,55]

$$P_{ave} = 0.0116 i_{corr} t \tag{23}$$

where time, t, is in years. ζ_{cc} is limited by the magnitude of the unconfined softening coefficient, such that if the theoretical value is lower than the experimental value for the unconfined section, then $\zeta_{cc} = \zeta_{uc}$. The effective confining pressure provided by the transverse reinforcement (K) can be determined through the work performed by Mander et al.,[52] updating the necessary material properties with their degraded counterparts

$$K = (1/2) k_e \rho_{sp,res} f_{yt,res} \tag{24}$$

$$k_e = \frac{1 - \dfrac{s}{2d_c}}{1 - \rho_{cc}} \tag{25}$$

$$\rho_{sp,res} = \frac{4A_{sp,res}}{d_c s} \tag{26}$$

where k_e is the confinement effectiveness coefficient; $\rho_{sp,res}$ is the residual transverse volumetric ratio; $A_{sp,res}$ and $f_{yt,res}$ can be determined using Eq. (9) and (10), respectively; s is

the spiral spacing; d_c is the diameter of the center-to-center enclosed spiral; and ρ_{cc} is the ratio of the longitudinal reinforcement area to the area of the confined core.

Uncracked concrete core—The compressive strength of the undamaged concrete core is affected only by the reduction in confinement effectiveness due to the degrading transverse steel and can, therefore, be represented as[52]

$$f_{cc} = \alpha_K f_c' \tag{27}$$

The measured crack patterns and parameters from Eq. (17) to (27) are presented in Appendix B.*

Mechanical modifications

Shear strut inclination—In the steel truss analogy proposed by Kowalsky and Priestley,[16] the angle of strut inclination to the column vertical axis (θ) is assumed to be 30 degrees. However, the angle gradually reduces as the increasing shear load causes a redistribution of imposed stresses.[13] A reliable theoretical derivation of the strut angle was developed by Ang[13] through plastic analyses using the mechanical degree of shear reinforcement.

$$\cot(\theta) = \sqrt{\frac{v - \psi}{\psi}} \tag{28}$$

$$\psi = \frac{\rho_{sp} f_{yt}}{f_c'} \tag{29}$$

where v is a web effectiveness factor to account for the concrete not developing full compressive strength. Recommended values of v range between 0.7 and 0.9.[56] Thürlimann et al.[57] presented kinematic limitations to the inclination of the compressive stress field of $0.5 \leq \tan(\theta) \leq 2.0$ or approximately 25 degrees $\leq \theta \leq$ 65 degrees, based on the achievable plastic strain distribution in concrete. The limit also ensures that the angle does not exceed a corner-to-corner failure plane of a column with an aspect ratio of less than 2.0.[13]

It was experimentally observed that corrosion enabled the exceedance of this kinematic limit, with strut angles measuring as low as 20.3 degrees. Geometrically, this is achieved by the inclusion of intermittent vertical cracks, so a strut can develop between the crack and neutral axis rather than fully developing to the extreme fiber (Fig. 4(b)). As corrosion damage increased, the average strut angle decreased (Table 2). Figure 5 presents the average strut inclination for both damage states as a function of mass loss. Angles presented in Table 2 and Fig. 5 were averaged over all significant diagonal shear cracks forming, measured digitally prior to cover spalling. In DS2, a plateauing occurred near approximately 25 degrees, while DS3 degraded slightly further, closer to 20 degrees. Neither CS-S1 nor CS-S2 developed significant diagonal cracks; instead, the concrete behavior was dominated by longitudinal bond damage originating from the existing corrosion damage. A probabilistic determination of the location and severity of corrosion cracking is outside the scope of this study; therefore, a conservative lower-bound estimate for the strut inclination is proposed based on each damage state, expressed by Eq. (30).

$$\theta' = \begin{cases} 25^\circ \text{ if DS2} \\ 20^\circ \text{ if DS3} \end{cases} \tag{30}$$

Neutral axis—As the unconfined concrete layer continually softens, the depth of the dependable compression block must be adjusted. When significantly pre-cracked, the idealized stress block of the concrete compressive section will nonlinearize, and the centroid of the compression zone will shift inward as the outer extremities soften and lose stiffness. At DS2, the applied compressive load should sufficiently offset the cover softening, closing minor cracks. A conservative estimate of the loss of section reliability can be represented as half the cover depth, resulting in a new equivalent section depth equal to $D - \delta$. At DS3, the cover is assumed to be generally unable to redistribute stresses between materials, resulting in an equivalent section depth equal to the depth of the enclosed concrete core (d).

Axial compression performance—Cracking through the concrete section has been shown experimentally to degrade the axial compressive strength of corroded RC columns.[5,58,59] Revathy et al.[59] observed a 3% and 12% decrease in the axial capacity of corroded RC circular columns for a longitudinal design mass loss of 10% and 25%, respectively. Based on these results, columns in the DS3 range likely experienced an actual axial load ratio closer to 0.05, potentially enhancing their shear performance compared with predictions. Based on the section model in Fig. 3, Campione et al.[5] proposed the following model to predict the degraded axial load-bearing capacity

$$P_{max,corr} = \psi_p f_c' A_{cover} + \psi_p f_{cc} A_{crackedcore} + f_{cc} A_{core} + A_l \sigma_s \tag{31}$$

where $A_l\sigma_s$ accounts for the reduction in longitudinal buckling resistance; A_{cover}, $A_{crackedcore}$, and A_{core} are derived from Fig. 3; and ψ_p is the ratio of the degraded compressive strength for each zone to the uncorroded compressive strength, proposed by Vecchio and Collins.[60] The reduction factor, ψ_p, derived through the Modified Compression Field Theory, is functionally equivalent to the softening coefficient, ζ.

The magnitude of the axial component (Eq. (3)) is determined by the horizontal component of the diagonal compression strut, which carries the shear stress from the application of axial force to the base of the column, illustrated in Fig. 4(c).[16] The axial component of the shear-resistance mechanism (Eq. (3) and Fig. 4(c)) is not directly analogous to the axial capacity (Eq. (31)). However, as the axial capacity declines, the shear resistance provided by the axial force is indirectly affected by the smaller dependable section. Thus, an equivalent relationship is proposed based on the dependable strength ($A_g f_c'$) of the deteriorated section.

*The Appendix is available at **www.concrete.org/publications** in PDF format, appended to the online version of the published paper. It is also available in hard copy from ACI headquarters for a fee equal to the cost of reproduction plus handling at the time of the request.

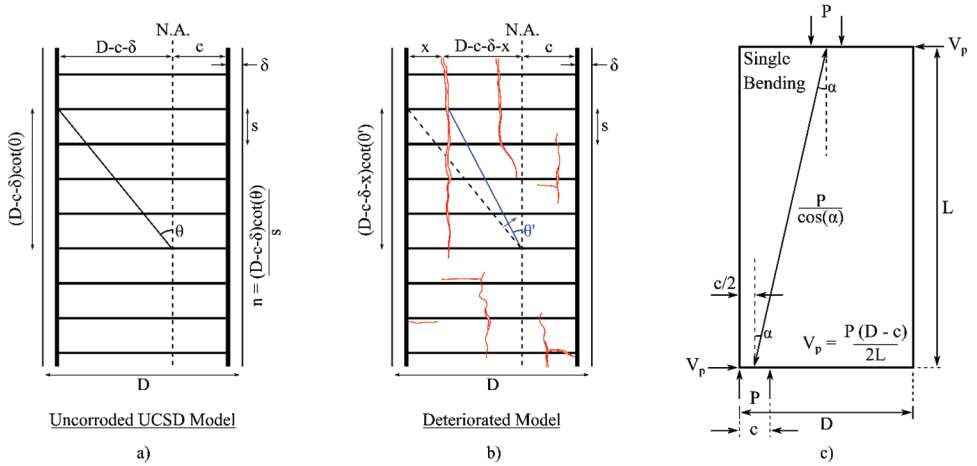

Fig. 4—(a) Original inclined strut-compression zone relationship; (b) change in strut formation with inclusion of vertical corrosion cracks; and (c) contribution of axial compressive load to shear capacity of RC column.[16]

$$D' = \begin{cases} \zeta_{uc}(D-d)+\zeta_{cc}(d-d')+d' & \text{if DS2} \\ \zeta_{cc}(d-d')+d' & \text{if DS3} \end{cases} \quad (32)$$

Displacement ductility—Four key points characterize the curve presented in Fig. 1(a): 1) the initial shear strength, $V_i(\gamma_i)$, before significant plasticity is reached; 2) the dependable displacement ductility limit, μ_i; 3) the flexural displacement ductility capacity, μ_f; and 4) the residual shear capacity, $V_f(\gamma_f)$, assumed to be reached once the displacement ductility $\mu_\Delta \geq \mu_f$. After exceeding μ_i (2.0 for an uncorroded column under uniaxial bending), the concrete shear resistance is assumed to degrade linearly due to excessive crack dilation. More participation is demanded from the yielding transverse reinforcement to compensate for the degradation in concrete strength, which can only be achieved by lowering the diagonal strut inclination of the analogous truss.[13] Hence, the extent of the degradation depends heavily upon the degree of core confinement. The greater the supplied transverse reinforcement and confinement, the later the onset of transverse yielding, leading to less degradation and larger displacement ductility.[18] The following sections propose estimations for deriving a member's design-specific shear-ductility envelope.

Shear strength before degradation, $V_{i,c}$—In an uncorroded state, $V_i = V_A$ (Eq. (1)) is related to the displacement ductility factor, γ_i, through Eq. (33).[14] Therefore, the reduced tensile strength of the concrete in a corroded state is related to the softened compressive strength by

$$f_{ct,corr} = 0.29\sqrt{\zeta_{uc} f_c'} \quad (33)$$

$$\gamma_i = 0.29\sqrt{\zeta_{uc}} \quad (34)$$

where ζ_{uc} governs both DS2 and DS3 zones because $\zeta_{uc} \leq \zeta_{cc}$.

Residual shear strength, $V_{f,c}$—The residual shear strength describes the level of underlying basic shear stress that can be sustained by sufficient confined strength.[13,14,23] $V_{f,c}$ is

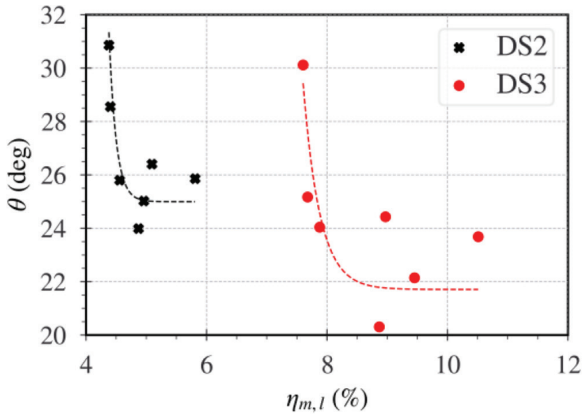

Fig. 5—Average measured shear strut angle for DS2 and DS3 test members.

obtained through the additive method in Eq. (1), accounting for the complete degradation of the concrete shear resistance

$$V_{f,c} = V_{sf,c} + V_{pf,c} + V_{cf,c} \quad (35)$$

V_{sf} is characterized by a change in strut angle to compensate for the degradation in concrete resistance. The lowered angle can be calculated using Eq. (28) and (29). From Ang,[13] the value of the web effectiveness factor, v, for a column failing in ductile flexural bending was calibrated to be 0.193. The residual axial component, V_{pf}, is assumed to keep the same form as Eq. (3). The residual concrete shear resistance is taken as

$$V_{cf} = v_{cf,c} A_e$$

$$V_{cf,c} = v_{cf,c} \cdot 0.8\left(\sqrt{\zeta_{uc}} A_{cover} + \sqrt{\zeta_{cc} \cdot \alpha_K} A_{crackedcore} + \sqrt{\alpha_K} A_{core}\right) \quad (36)$$

where the concrete shear stress, v_{cf}, is taken as half of the basic shear stress, $v_b = 0.37\sqrt{f_c'}$ (for $\rho_l \geq 1.3\%$), if the section is sufficiently confined.[18] It can be empirically assumed that

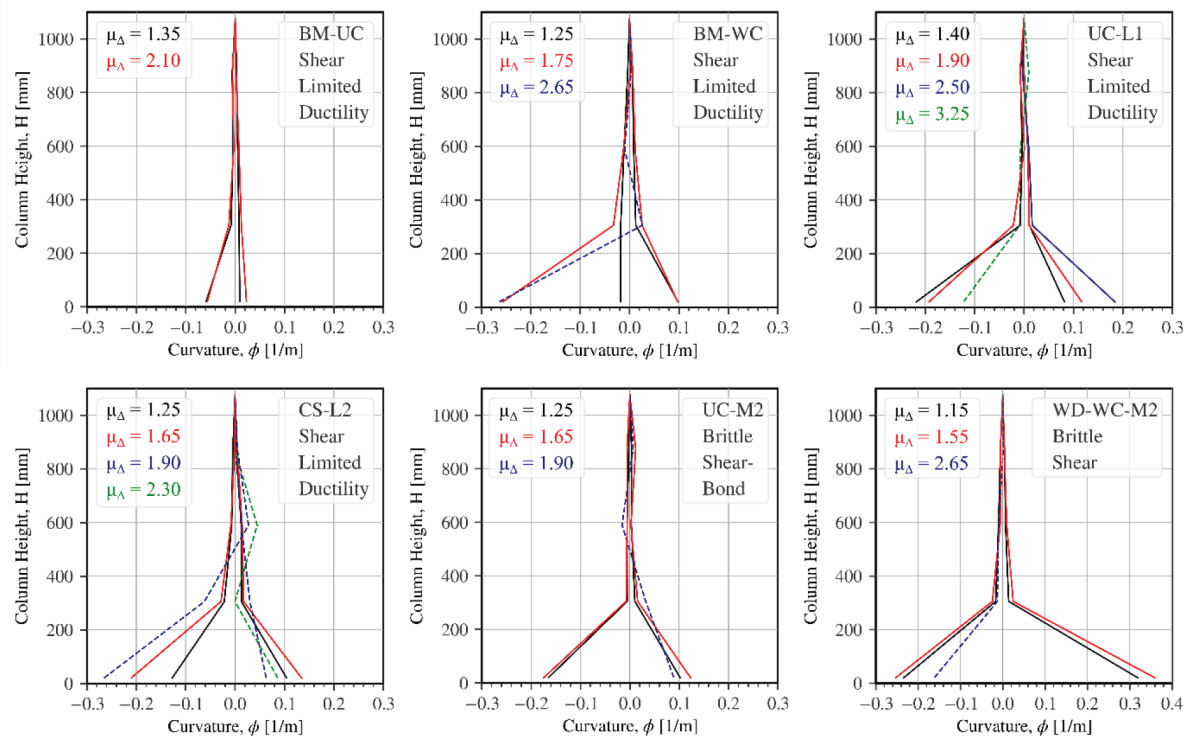

Fig. 6—Curvature profiles for uncorroded benchmark specimens (BM-UC and BM-WC); typical curvature profiles of DS2 members (UC-L1 and CS-L2); and DS3 columns (UC-M2 and UC-S1).

$$v_{cf,c} = \begin{cases} 0.185\sqrt{\zeta_{uc} f_c'} & \text{if } \rho_{sp,res} \geq 1\% \\ 18.5\rho_{sp,res}\sqrt{\zeta_{uc} f_c'} & \text{if } \rho_{sp,res} < 1\% \end{cases} \quad (37)$$

Assuming that the confined concrete core can still provide a fragment of aggregate interlock at high displacement ductility (Eq. (36)), the Kowalsky and Priestley[16] base limit of $\gamma_f = 0.05$ can be maintained as a reasonable lower-bound estimate.

Dependable displacement ductility, μ_i—The dependable displacement ductility, μ_i, defined by the onset of degrading concrete shear resistance due to accumulative plasticity and loss of aggregate interlock, is taken as 2.0 for a column in an uncorroded state.[13] Due to increased bond damage and bond-slip in corroded members, less energy is dissipated for the same lateral deflection measured in an equivalent uncorroded member. Furthermore, because the elastoplastic yield displacement is defined by the secant stiffness of the force-displacement response at $0.75P_{peak}$,[61] some curvature is experienced (initial yielding of the outer bars) before complete yield is achieved (characteristic of circular cross sections). Therefore, because a larger proportion of the lateral deflection is attributed to bond-slip in corroded situations, less energy is being dissipated at the same lateral deflection, and the actual displacement ductility due to yielding of the longitudinal bars is reduced, ultimately causing a reduction in the dependable displacement ductility.

When shear deformations begin to dominate the performance, the curvature profiles along the member height tend to become more irregular.[13] Thus, $\mu_i = 2$ describes the final ductility at which curvature regularity is maintained, which characterizes the transition in failure from shear with limited ductility ($2 < \mu \leq 4$) to brittle shear ($1 < \mu \leq 2$) (Fig. 6). Therefore, the degradation of the dependable displacement ductility limit can be qualitatively estimated through a curvature assessment of columns under corroded conditions. It is assumed that all members failing in brittle modes (DS3) do not achieve the dependable ductility limit before reaching μ_Δ, which serves as a conservative lower-bound estimate and forms the scope of this analysis to $\mu_c \leq \mu < 2.0$.

Figure 6 presents example curvature profiles for DS0, DS2, and DS3 specimens. For DS2 members failing with limited ductility, the minimum measured ductility at which an irregular curvature distribution was recorded was found to be $\mu = 1.7$. In DS3, where all members failed in brittle modes, the maximum ductility that maintained a regular curvature profile was determined to be 1.7, with an average of 1.5. Therefore, a conservative lower-bound estimate of $\mu_i = 1.5$ was adopted for members within DS3.

$$\mu_{i,c} = \begin{cases} 1.70 \text{ if DS2} \\ 1.50 \text{ if DS3} \end{cases} \quad (38)$$

The initial assumption that all ductilities over $\mu = 2.0$ initiate degradation of the concrete shear resistance is also qualitatively verified by the uncorroded curvature profiles in Fig. 6.

Flexural ductility capacity, μ_f—The flexural displacement ductility capacity, μ_f, describes the ductility required to ensure a pure bending failure with no shear influence (Fig. 1(a)). The UCSD model considers $\mu_f = 8.0$. To characterize an equivalent degraded flexural displacement ductility factor, $\mu_{f,c}$, a database of 44 additional circular columns tested

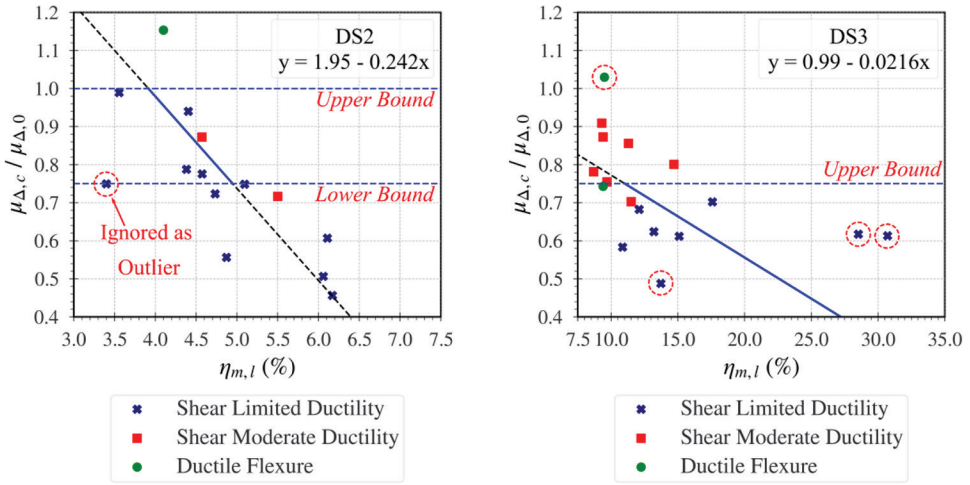

Fig. 7—Displacement ductility degradation with increasing corrosion damage using data collected from literature.[6,8,30-32,62]

under quasi-static lateral cyclic loading was compiled from six research programs.[6,8,30-32,62] Ductility capacities, aspect ratios, and longitudinal mass losses ranged between $1.31 \le \mu \le 11.9$, $2.0 \le L/D \le 6.0$, and $0 \le \eta_{m,l} \le 30.71\%$, respectively.

A degradation relationship was derived between the normalized displacement ductility capacity ($\mu_{\Delta,c}/\mu_{\Delta,0}$) and $\eta_{m,l}$ for the DS2 and DS3 zones, shown in Fig. 7. All tests failing in brittle modes without developing notable ductility were removed from the regression analysis. The linear regressions for DS2 and DS3 are given by Eq. (39) (Fig. 7).

$$\mu_{\Delta,c} = \begin{cases} 0.75 \le (1.95 - 0.2419\eta_{m,l})\mu_{\Delta,0} \le 1.0 \text{ if DS2} \\ (0.99 - 0.0216\eta_{m,l})\mu_{\Delta,0} \le 0.75 \text{ if DS3} \end{cases} \quad (39)$$

Thus, the degraded flexural ductility capacity, $\mu_{f,c}$, can be determined by substituting $\mu_{f,0} = 8.0$ into Eq. (39). The imposed limits, $0.75 <$ DS2 ≤ 1.0 and DS3 ≤ 0.75, ensure continuity between damage states. The Eq. (39) regression produced predictions with an R^2 of 0.850 and 0.768 for DS2 and DS3, respectively, with calculated MAPEs of 13.9% and 21.4%.

Bond failure penalization

Brittle shear-bond failures are characterized by severe bond cracking through the concrete cover, originating from longitudinal corrosion cracks, which influences the initial loss of concrete strength at the point of spalling (often at the peak load). Shear failure is then distinguished by the rupture of the spiral reinforcement, resulting in an acute drop in load-bearing strength as the steel contribution is abruptly lost. In a member failing in shear-bond, diagonal struts cannot adequately develop due to significant vertical cracking (Fig. 4(b)), redistributing imposed stresses immediately after loading begins—that is, the concrete has no opportunity to establish the desirable inclined stress pathways. Thus, the maximum shear resistance of the transverse steel cannot be fully developed. Table 2 shows that those members failing with bond characteristics typically demonstrated greater losses in peak shear capacity relative to the uncorroded benchmarks. The maximum crack width

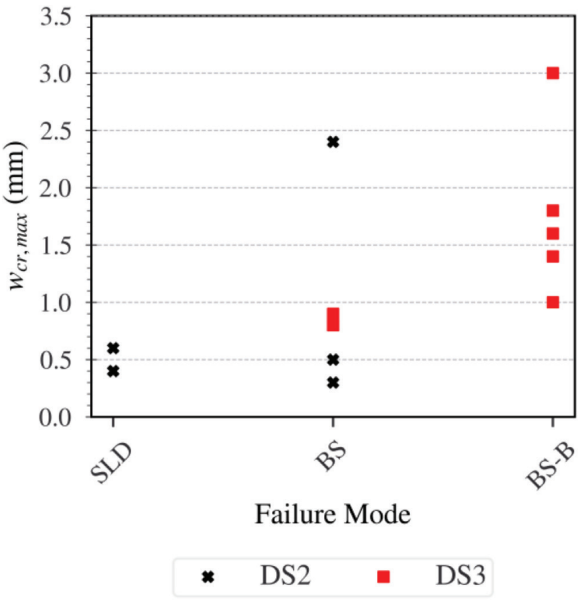

Fig. 8—Maximum crack width and transition in failure mode. (Note: SLD is shear limited ductility; BS is brittle shear; BS-B is brittle shear-bond.)

($w_{cr,max}$) provides the strongest correlation to the onset of bond-oriented failure modes, as shown in Fig. 8. Excluding specimen WD-WC-M1, a threshold maximum crack width of 1.0 mm within the DS3 range signifies the onset of bond cracks dominating the concrete performance. Hence, a penalization factor, ψ_B, is proposed for those members whose concrete resistance is lost prematurely through bond before the complete shear resistance can be developed.

$$\psi_B = \begin{cases} 1.0 \text{ if DS2} \\ 1.0 \text{ if DS3 and } w_{cr,max} < 1.0 \text{ mm} \\ 0.85 \text{ if DS3 and } w_{cr,max} \ge 1.0 \text{ mm} \end{cases} \quad (40)$$

Crack correction factor

At low corrosion, concrete resistance is overly penalized by softening coefficients of $\zeta < 0.75$. Given the same initial concrete compressive strength, a 20% reduction in V_c is measured between BM-WC and WD-WC-L1 ($\eta_{m,l} = 4.38\%$).

The increased crack area is more likely to supply a small compensatory effect, whereby the early redistribution of stress provides a greater opportunity for aggregate interlock, dowel action, and shear transfer before significant deflection is reached. This effect would be an amplification of the concrete shear resistance (before exceeding μ_i), based on the total crack strain and remaining confining steel volume.

Another important consideration is the documented effect of corrosion rate on morphology and crack growth.[63,64] Larger current densities are known to increase the likelihood of uniformly distributed corrosion patterns while decreasing the frequency of localized pitting, which is characteristic of naturally occurring corrosion.[65] A corrosion rate correction is therefore proposed to account for the relationship between crack growth and the rate of material loss per year (Ri_{corr}). An empirical correction factor, v_c, is proposed in the following form

$$1.0 \leq v_c = 1.05 + \frac{\varepsilon_{cr}}{\frac{L}{D} \cdot \rho_{sp,res}} - (R\,i_{corr})^2 \leq 1.3 \quad (41)$$

$$R(i) = \frac{A}{ZF\gamma_{Fe}} \quad (42)$$

Current density is measured relative to the actual impressed time for those subjected to wetting-and-drying cycles. A is the molar mass of iron (55.847 g); Z is the ionic valency of iron (2); F is Faraday's constant (96,487 A·s); and γ_{Fe} is the density of iron (7.86 g/cm^3). Hence, the material loss per year for a given current density is $R(i)$ = 1161.1 cm/year.

MODELING RESULTS

Table 3 presents the results of models *M*-0 to *M*-3. A summary of model *M*-3 is presented in Appendix C. Model *M*-0 accurately estimated the peak shear capacity of columns within the DS2 range while underpredicting the uncorroded benchmark members and drastically overpredicting severely deteriorated members. An important observation is the substantial increase in test variability at higher levels of corrosion (DS3) compared to DS2. Given similar corroded properties, there is considerable variation in the experimental test performances within the DS3 range. For example, UC-M1 and UC-S1 had measured peak capacities of 588 and 495 kN (16% variance), respectively, with average transverse mass losses of $\eta_{m,sp}$ = 3.75% and 43.0%, respectively. Observations taken during testing show that the corrosion damage location becomes a critical parameter at larger deterioration when considered relative to the load direction. The likely reason UC-M1 performed so well was that most of the corrosion damage was located outside of the shear planes and was more heavily concentrated toward the push-pull extreme fibers. The location and distribution of the corrosion damage relative to the load direction were not adequately captured by an average mass loss measurement, which is the prevailing measurement of experimental corrosion. Therefore, to account for test variance and improve model predictions, a distribution parameter considering the global distribution with respect to the location of the shear planes would be required. Global corrosion distribution was not quantitatively measured in the program presented in this work, so a location parameter must be considered in future research.

Figure 9 compares the predictive performance of each model against the measured experimental capacity. The final *M*-3 model efficiently estimates the peak shear capacity, particularly within the DS3 range. All but two test specimens (WD-WC-S1 and WD-WC-S2) were conservatively underpredicted, with a mean prediction ratio of 8.60%. DS2 predictions demonstrated a strong model consistency with a variance of 5.53%. The predictions were still conservative, however, with a mean ratio of 13.13%. This is likely the result of over-penalizing the steel truss component, with transverse mass losses ranging between 12.7 and 28.8%. Despite the relatively high transverse deterioration, DS2 columns still performed exceptionally well compared to their uncorroded counterparts. Models *M*-1 and *M*-2 showed high scatter and poor predictive accuracy. Therefore, models *M*-1 and *M*-2 are unsuitable predictive tools for the degraded cyclic shear capacity of corroded shear-critical RC circular columns.

From Fig. 9(e), the effect of the crack enhancement on the prediction ratio can be seen to have a mild negative trend, thus justifying the need to impose limits on Eq. (39), which may be iteratively improved as more data become available. Figure 10 illustrates the shear-ductility envelopes of a selection of test specimens from each damage state, highlighting the change in slope as a function of design and corrosion damage. Additional verification should be sought for the proposed modifications to the displacement ductility curve, implementing force-displacement responses and numerical analyses over a greater range of ductility capacities and failure modes.

Finally, to ensure that all predictions provide a conservative prediction of the actual shear capacity, a strength reduction design factor is proposed based on Table 3 in the form of

$$V_{D,c} = \phi V_{A,c} \quad (43)$$

$$\phi = 0.80$$

CONCLUSIONS AND LIMITATIONS

An adaptation of an existing analytical model for calculating the cyclic shear capacity of circular reinforced concrete (RC) columns, considering the effects of chloride-induced corrosion, is presented in this research. The modifications account for material and mechanical degradation effects within the corroded RC column. The proposed model categorizes RC columns by the severity of the corrosion damage, represented as different damage states. Damage states 0 (DS0) and 1 (DS1) represent effective uncorroded conditions, so the model maintains its original structure. DS2 and DS3 describe moderately to severely corroded states, defined by the average longitudinal mass loss ranges of $1.5\% < \eta_{m,l} \leq 7.5\%$ and $\eta_{m,l} > 7.5\%$, where 7.5% longitudinal mass loss corresponds to approximately 27.5% average transverse mass loss. New empirical decay law coefficients are proposed to explain the reduction in material properties with increasing corrosion based on a database of over 1380 corroded tensile tests.

Table 3—Models *M*-0 to *M*-3 results and comparison with experimental values, ordered by ascending longitudinal mass loss

Damage state	Specimen ID	$\eta_{m,l}$, %	$V_{max,exp}$	$V_{A,M\text{-}0}$	$V_{A,M\text{-}1}$	$V_{A,M\text{-}2}$	$V_{A,M\text{-}3}$	$V_{max,exp}/V_{A,M\text{-}0}$	$V_{max,exp}/V_{A,M\text{-}1}$	$V_{max,exp}/V_{A,M\text{-}2}$	$V_{max,exp}/V_{A,M\text{-}3}$
DS0	BM-UC	0.00	499.8	470.0	—	—	—	1.06	—	—	—
	BM-WC	0.00	689.0	618.9	—	—	—	1.11	—	—	—
	Mean							**1.09**	—	—	—
	Mean, %							**8.83**	—	—	—
	Std., %							**3.54**	—	—	—
DS2	WD-WC-L1	4.38	764.3	705.3	659.3	579.8	665.3	1.08	1.16	1.32	1.15
	WD-WC-L2	4.40	636.8	632.0	590.3	477.8	591.0	1.01	1.08	1.33	1.08
	UC-L2-2.95	4.56	498.2	503.9	467.7	438.1	451.0	0.99	1.07	1.14	1.10
	UC-L1	4.87	512.7	511.6	468.8	442.0	472.4	1.00	1.09	1.16	1.09
	CS-WC-L1	4.96	671.0	705.3	643.9	544.1	613.5	0.95	1.04	1.23	1.09
	CS-WC-L2	5.10	680.0	667.5	606.0	515.5	569.3	1.02	1.12	1.32	1.19
	WD-WC-M1	5.81	670.8	705.3	621.3	477.2	552.4	0.95	1.08	1.41	1.21
	Mean							**1.00**	**1.09**	**1.27**	**1.13**
	Mean, %							**0.05**	**9.15**	**27.23**	**13.13**
	Std., %							**4.53**	**3.87**	**9.85**	**5.53**
DS3	WD-WC-S2	7.61	492.7	667.5	542.9	413.3	522.8	0.74	0.91	1.19	0.94
	WD-WC-M2	7.68	706.1	663.5	537.8	444.8	597.0	1.06	1.31	1.59	1.18
	UC-M1	7.88	587.8	509.9	409.4	375.3	444.4	1.15	1.44	1.57	1.32
	WD-WC-S1	8.87	430.4	705.3	540.0	445.3	539.4	0.61	0.80	0.97	0.80
	UC-M2	8.97	477.8	511.1	389.3	398.1	432.6	0.93	1.23	1.20	1.10
	UC-S2-2.95	9.45	390.9	503.9	374.7	383.1	390.8	0.78	1.04	1.02	1.00
	UC-S1	10.5	494.9	509.9	358.8	367.5	435.4	0.97	1.38	1.35	1.14
	CS-WC-S2	12.8	507.0	705.3	434.7	409.0	452.7	0.72	1.17	1.24	1.12
	CS-WC-S1	13.2	518.0	705.3	424.5	398.9	443.8	0.73	1.22	1.30	1.17
	Mean							**0.86**	**1.17**	**1.27**	**1.09**
	Mean, %							**–14.45**	**16.55**	**26.86**	**8.60**
	Std., %							**18.20**	**21.34**	**21.26**	**15.29**

Note: A negative mean prediction represents a mean prediction ratio less than 1.0; Std. is standard deviation.

The changes in diagonal strut inclination, degradation of axial compression capacity, neutral axis depth, the relationship between concrete shear resistance and displacement ductility, bond degradation, and shear stress transfer through concrete cracking are considered in the model. An additional database of 44 corroded circular columns is compiled to derive new shear-ductility relationships for each corroded damage state.

The final proposed model was shown to improve the predictive performance and variance compared to simplified degradation models developed for comparison, particularly in more severely corroded ranges (DS3). Due to the limited experimental data available on corroded RC circular columns failing in shear-dominated modes, a degree of scatter remains in the final model. It was observed that the prevailing location of the corrosion damage relative to the load direction (and, therefore, the formation of shear planes) heavily dictated the final performance. Thus, a corrosion distribution parameter relative to the shear planes should be explored to account for test variance and improve the final model predictions. Global corrosion distribution was not quantitatively measured in the experimental program presented in this work, so a location parameter must be considered in future research. Nevertheless, with a mean predictive ratio of ±8.60% compared to the experimental data, the model provides a strong predictive tool for the assessment of aging and compromised RC columns subjected to chloride-induced deterioration. Final DS2 predictions demonstrated a conservative mean predictive accuracy of +13.13%. Through a comprehensive comparison between the original model, two simplified degradation models, and the final proposed model, the original (uncorroded) model proposed by Kowalsky and Priestley[16] provided the strongest predictive accuracy for columns within the DS2 range, with a mean accuracy of 0.05% and a standard deviation of 4.53%.

Although many of the proposed modifications involve well-founded concepts from the literature, the final proposed

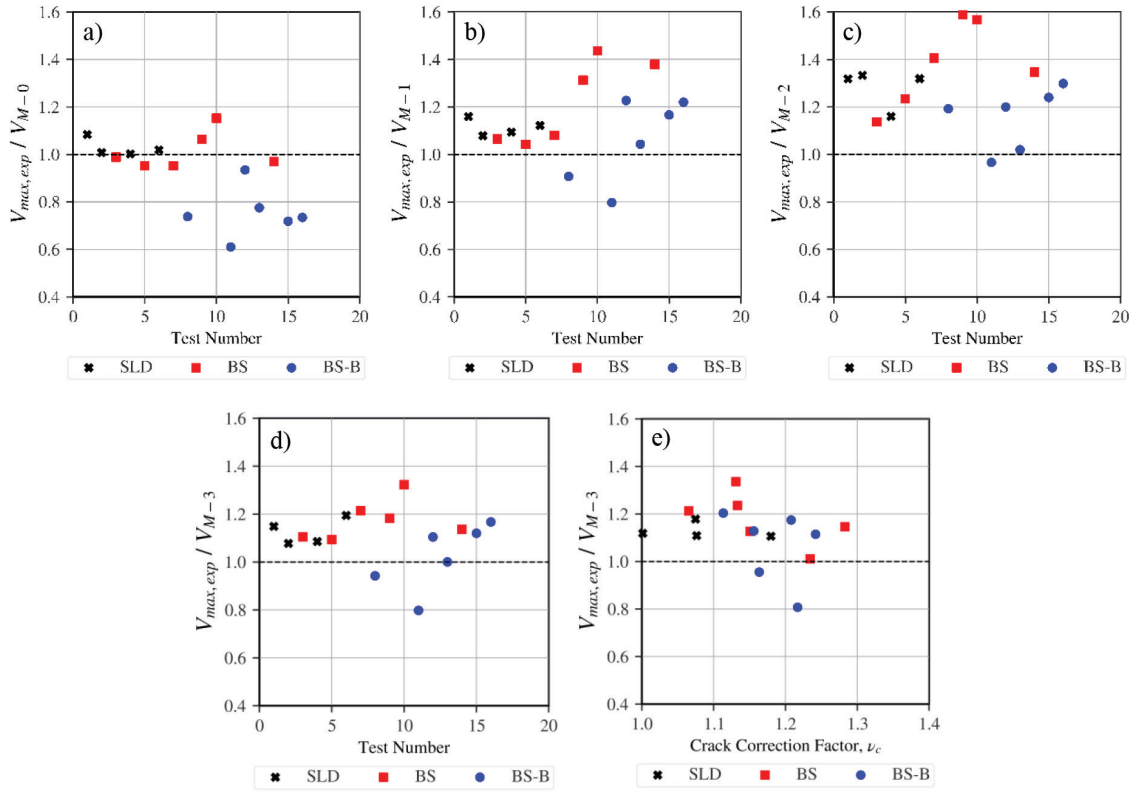

Fig. 9—(a) Model M-*0 prediction results compared with experimental results; (b)* M-*1; (c)* M-*2; (d)* M-*3; and (e) influence of crack correction factor on model* M-*3 predictions. (Note: SLD is shear limited ductility; BS is brittle shear; BS-B is brittle shear-bond.)*

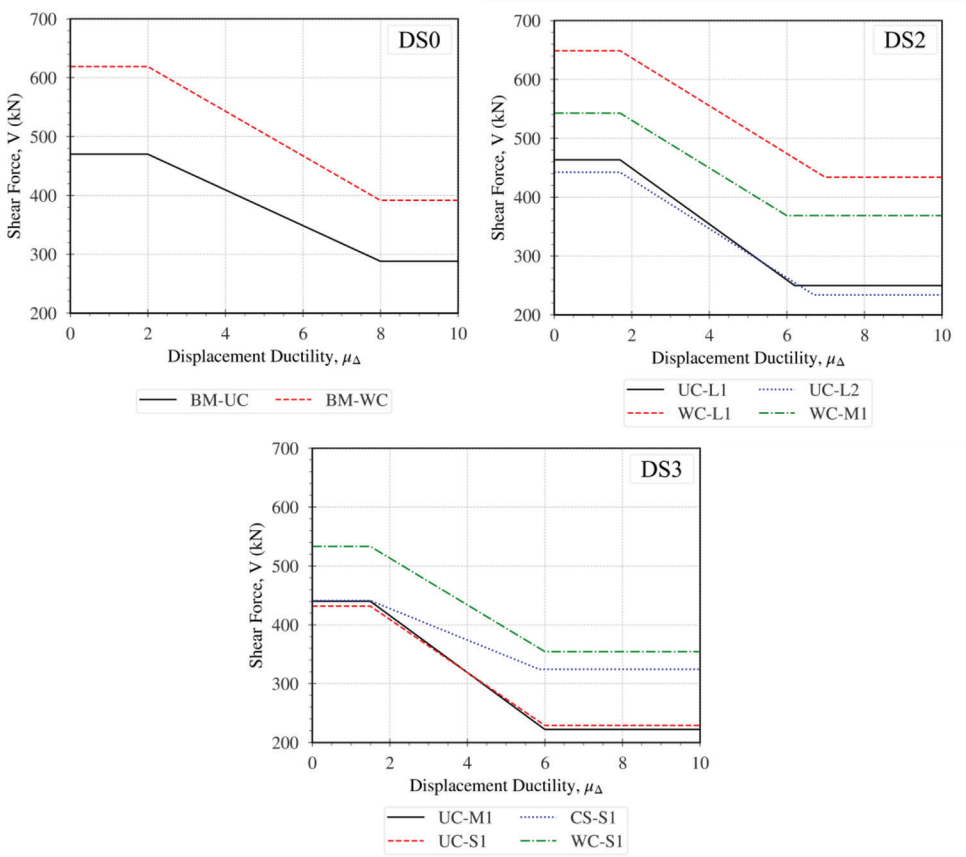

Fig. 10—Example shear capacity-ductility envelopes for several DS0, DS2, and DS3 members based on design and corrosion properties.

model was built upon a limited pool of data, considering only a small range of aspect ratios, confinement degrees, failure modes, and one axial load ratio. More testing must be conducted across key experimental variables to improve predictive ability.

AUTHOR BIOS

Benjamin Matthews *is a Postdoctoral Researcher at Eindhoven University of Technology, Eindhoven, the Netherlands. He received his PhD in civil engineering from the University of Canterbury, Christchurch, New Zealand, in 2023. His PhD research focused on the assessment of reinforcement corrosion in aged structures, predictive machine-learning applications, and the seismic shear performance of reinforced concrete (RC) bridge piers. His research interests include the reuse of existing precast concrete elements and their applications in new designs.*

ACI member **Alessandro Palermo** *is a Professor in the Department of Structural Engineering at the University of California, San Diego, La Jolla, CA, previously at the University of Canterbury. He received his BS, MS, and PhD in civil engineering from the Polytechnic University of Milan, Milan, Italy, in 1997, 1999, and 2004, respectively. His research interests include the seismic behavior of RC structures, including novel materials, long-term seismic resilience and corrosion effects, and nonmetallic reinforcement.*

Allan Scott *is an Associate Professor of civil engineering in the Civil and Natural Resources Engineering Department at the University of Canterbury. He received his BEng from McMaster University, Hamilton, ON, Canada, and his master's and PhD from the University of Cape Town, Cape Town, South Africa, in 1994, 1997, and 2004, respectively. His research interests include the development of sustainable construction materials, assessment of the residual capacity of corroded and seismically damaged RC structures, and in-place resource use options for off-Earth civil engineering construction applications.*

ACKNOWLEDGMENTS

The authors would like to acknowledge the Civil and Natural Resources Engineering Department and the University of Canterbury Structural Engineering Laboratory technical staff for their contributions and financial support, without whom this work would not be possible.

REFERENCES

1. Bertolini, L.; Elsener, B.; Pedeferri, P.; Redaelli, E.; and Polder, R. B., *Corrosion of Steel in Concrete: Prevention, Diagnosis, Repair*, second edition, Wiley-VCH Verlag GmbH & Co. KGaA, Weinheim, Germany, 2013, 434 pp.

2. Ye, H.; Fu, C.; Tian, Y.; and Jin, N., *Chloride-Induced Steel Corrosion in Concrete Under Service Loads*, Springer, Singapore, 2020, 138 pp.

3. Apostolopoulos, C. A., and Papadopoulos, M. P., "Tensile and Low Cycle Fatigue Behavior of Corroded Reinforcing Steel Bars S400," *Construction and Building Materials*, V. 21, No. 4, Apr. 2007, pp. 855-864. doi: 10.1016/j.conbuildmat.2005.12.012

4. Melchers, R. E., "Long-Term Durability of Marine Reinforced Concrete Structures," *Journal of Marine Science and Engineering*, V. 8, No. 4, Apr. 2020, Article No. 290. doi: 10.3390/jmse8040290

5. Campione, G.; Cannella, F.; and Minafò, G., "A Simple Model for the Calculation of the Axial Load-Carrying Capacity of Corroded RC Columns," *Materials and Structures*, V. 49, No. 5, May 2016, pp. 1935-1945. doi: 10.1617/s11527-015-0624-4

6. Ma, Y.; Che, Y.; and Gong, J., "Behavior of Corrosion Damaged Circular Reinforced Concrete Columns Under Cyclic Loading," *Construction and Building Materials*, V. 29, Apr. 2012, pp. 548-556. doi: 10.1016/j.conbuildmat.2011.11.002

7. Guo, A.; Li, H.; Ba, X.; Guan, X.; and Li, H., "Experimental Investigation on the Cyclic Performance of Reinforced Concrete Piers with Chloride-Induced Corrosion in Marine Environment," *Engineering Structures*, V. 105, Dec. 2015, pp. 1-11. doi: 10.1016/j.engstruct.2015.09.031

8. Andisheh, K., "Seismic Performance of Corroded Reinforced Concrete Bridge Piers," PhD thesis, University of Canterbury, Christchurch, New Zealand, 2017, 220 pp.

9. Rajput, A. S., and Sharma, U. K., "Corroded Reinforced Concrete Columns Under Simulated Seismic Loading," *Engineering Structures*, V. 171, Sept. 2018, pp. 453-463. doi: 10.1016/j.engstruct.2018.05.097

10. Palsson, R., and Mirza, M. S., "Mechanical Response of Corroded Steel Reinforcement of Abandoned Concrete Bridge," *ACI Structural Journal*, V. 99, No. 2, Mar.-Apr. 2002, pp. 157-162.

11. Dasar, A.; Hamada, H.; Sagawa, Y.; and Yamamoto, D., "Deterioration Progress and Performance Reduction of 40-Year-Old Reinforced Concrete Beams in Natural Corrosion Environments," *Construction and Building Materials*, V. 149, Sept. 2017, pp. 690-704. doi: 10.1016/j.conbuildmat.2017.05.162

12. Millard, S. G., and Johnson, R. P., "Shear Transfer Across Cracks in Reinforced Concrete due to Aggregate Interlock and to Dowel Action," *Magazine of Concrete Research*, V. 36, No. 126, Mar. 1984, pp. 9-21. doi: 10.1680/macr.1984.36.126.9

13. Ang, B. G., "Seismic Shear Strength of Circular Bridge Piers," PhD thesis, University of Canterbury, Christchurch, New Zealand, 1985, 439 pp.

14. Priestley, M. J. N.; Verma, R.; and Xiao, Y., "Seismic Shear Strength of Reinforced Concrete Columns," *Journal of Structural Engineering*, ASCE, V. 120, No. 8, Aug. 1994, pp. 2310-2329. doi: 10.1061/(ASCE)0733-9445(1994)120:8(2310)

15. ACI Committee 318, "Building Code Requirements for Structural Concrete (ACI 318-19) and Commentary (ACI 318R-19) (Reapproved 2022)," American Concrete Institute, Farmington Hills, MI, 2019, 624 pp.

16. Kowalsky, M. J., and Priestley, M. J. N., "Improved Analytical Model for Shear Strength of Circular Reinforced Concrete Columns in Seismic Regions," *ACI Structural Journal*, V. 97, No. 3, May-June 2000, pp. 388-396.

17. Joint ASCE-ACI Task Committee 426, "The Shear Strength of Reinforced Concrete Members," *Journal of the Structural Division*, ASCE, V. 99, No. 6, June 1973, pp. 1091-1187.

18. Ang, B. G.; Priestley, M. J. N.; and Paulay, T., "Seismic Shear Strength of Circular Reinforced Concrete Columns," *ACI Structural Journal*, V. 86, No. 1, Jan.-Feb. 1989, pp. 45-59.

19. Wong, Y.-L.; Paulay, T.; and Priestley, M. J. N., "Response of Circular Reinforced Concrete Columns to Multi-Directional Seismic Attack," *ACI Structural Journal*, V. 90, No. 2, Mar.-Apr. 1993, pp. 180-191.

20. Aschheim, M., and Moehle, J. P., "Shear Strength and Deformability of RC Bridge Columns Subjected to Inelastic Cyclic Displacements," Report No. UCB/EERC-92/04, Earthquake Engineering Research Center, University of California, Berkeley, Berkeley, CA, Mar. 1992, 114 pp.

21. Caltrans, "Earthquake Retrofit Analysis for Single Column Bents," Caltrans Memo to Designers 20-4, Attachment B, California Department of Transportation, Sacramento, CA, 1996.

22. ATC, "Improved Seismic Design Criteria for California Bridges: Provisional Recommendations," Report No. ATC-32, Applied Technology Council, Redwood City, CA, 1996, 240 pp.

23. NZS 3101.1&2:2006, "Concrete Structures Standard," Standards New Zealand, Wellington, New Zealand, 2006, 754 pp.

24. Cai, G.; Sun, Y.; Takeuchi, T.; and Zhang, J., "Proposal of a Complete Seismic Shear Strength Model for Circular Concrete Columns," *Engineering Structures*, V. 100, Oct. 2015, pp. 399-409. doi: 10.1016/j.engstruct.2015.06.032

25. Göksu, Ç., "Seismic Behavior of RC Columns with Corroded Plain and Deformed Reinforcing Bars," PhD thesis, Istanbul Technical University, Istanbul, Turkey, 2012, 540 pp.

26. Meda, A.; Mostosi, S.; Rinaldi, Z.; and Riva, P., "Experimental Evaluation of the Corrosion Influence on the Cyclic Behaviour of RC Columns," *Engineering Structures*, V. 76, Oct. 2014, pp. 112-123. doi: 10.1016/j.engstruct.2014.06.043

27. Ma, G.; Li, H.; and Hwang, H.-J., "Seismic Behavior of Low-Corroded Reinforced Concrete Short Columns in an over 20-Year Building Structure," *Soil Dynamics and Earthquake Engineering*, V. 106, Mar. 2018, pp. 90-100. doi: 10.1016/j.soildyn.2017.12.006

28. Dai, K.-Y.; Lu, D.-G.; and Yu, X.-H., "Experimental Investigation on the Seismic Performance of Corroded Reinforced Concrete Columns Designed with Low and High Axial Load Ratios," *Journal of Building Engineering*, V. 44, Dec. 2021, Article No. 102615. doi: 10.1016/j.jobe.2021.102615

29. Zhao, J.; Lin, Y.; Li, X.; and Meng, Q., "Experimental Study on the Cyclic Behavior of Reinforced Concrete Bridge Piers with Non-Uniform Corrosion," *Structures*, V. 33, Oct. 2021, pp. 999-1006.

30. Yuan, W.; Guo, A.; and Li, H., "Experimental Investigation on the Cyclic Behaviors of Corroded Coastal Bridge Piers with Transfer of Plastic Hinge due to Non-uniform Corrosion," *Soil Dynamics and Earthquake Engineering*, V. 102, Nov. 2017, pp. 112-123. doi: 10.1016/j.soildyn.2017.08.019

31. Feng, R.; Zhang, J.; Li, Y.; and Zhu, J.-H., "Experimental Study on Hysteretic Behavior for Corroded Circular RC Columns Retrofitted by ICCP-SS," *Structures*, V. 35, Jan. 2022, pp. 421-435. doi: 10.1016/j.istruc.2021.10.039

32. Li, Y.; Zheng, S.; Shang, Z.; Chen, J.; and Wang, D., "Experimental Study on the Seismic Behavior of ECE Corroded Reinforced Concrete Short Pier Columns," *Construction and Building Materials*, V. 348, Sept. 2022, Article No. 128681. doi: 10.1016/j.conbuildmat.2022.128681

33. Li, Y.; Sun, Z.; Li, Y.; Zhu, W.; Zheng, H.; and Zheng, S., "Exploring the Shear Performance and Predictive Shear Capacity of Corroded RC Columns Utilizing the Modified Compression-Field Theory: An Investigative Study," *Engineering Structures*, V. 302, Mar. 2024, Article No. 117390. doi: 10.1016/j.engstruct.2023.117390

34. Matthews, B.; Palermo, A.; and Scott, A., "Cyclic Shear Testing of Artificially Corroded Reinforced Concrete Short Circular Piers," *Structures*, V. 63, May 2024, Article No. 106275. doi: 10.1016/j.istruc.2024.106275

35. ACI Innovation Task Group 1, "Acceptance Criteria for Moment Frames Based on Structural Testing (ACI T1.1-01) and Commentary (ACI T1.1R-01)," American Concrete Institute, Farmington Hills, MI, 2001, 10 pp.

36. Imperatore, S., "Mechanical Properties Decay of Corroded Reinforcement in Concrete—An Overview," *Corrosion and Materials Degradation*, V. 3, No. 2, June 2022, pp. 210-220. doi: 10.3390/cmd3020012

37. Cairns, J.; Plizzari, G. A.; Du, Y.; Law, D. W.; and Franzoni, C., "Mechanical Properties of Corrosion-Damaged Reinforcement," *ACI Materials Journal*, V. 102, No. 4, July-Aug. 2005, pp. 256-264.

38. Du, Y. G.; Clark, L. A.; and Chan, A. H. C., "Residual Capacity of Corroded Reinforcing Bars," *Magazine of Concrete Research*, V. 57, No. 3, Apr. 2005, pp. 135-147. doi: 10.1680/macr.2005.57.3.135

39. Lee, H.-S., and Cho, Y.-S., "Evaluation of the Mechanical Properties of Steel Reinforcement Embedded in Concrete Specimen as a Function of the Degree of Reinforcement Corrosion," *International Journal of Fracture*, V. 157, No. 1-2, May 2009, pp. 81-88. doi: 10.1007/s10704-009-9334-7

40. Ou, Y.-C.; Susanto, Y. T. T.; and Roh, H., "Tensile Behavior of Naturally and Artificially Corroded Steel Bars," *Construction and Building Materials*, V. 103, Jan. 2016, pp. 93-104. doi: 10.1016/j.conbuildmat.2015.10.075

41. Imperatore, S.; Rinaldi, Z.; and Drago, C., "Degradation Relationships for the Mechanical Properties of Corroded Steel Rebars," *Construction and Building Materials*, V. 148, Sept. 2017, pp. 219-230. doi: 10.1016/j.conbuildmat.2017.04.209

42. Fernandez, I., and Berrocal, C. G., "Mechanical Properties of 30 Year-Old Naturally Corroded Steel Reinforcing Bars," *International Journal of Concrete Structures and Materials*, V. 13, No. 1, Dec. 2019, Article No. 9. doi: 10.1186/s40069-018-0308-x

43. Vanama, R. K., and Ramakrishnan, B., "Improved Degradation Relations for the Tensile Properties of Naturally and Artificially Corroded Steel Rebars," *Construction and Building Materials*, V. 249, July 2020, Article No. 118706. doi: 10.1016/j.conbuildmat.2020.118706

44. Almusallam, A. A.; Al-Gahtani, A. S.; Aziz, A. R.; and Rasheeduzzafar, "Effect of Reinforcement Corrosion on Bond Strength," *Construction and Building Materials*, V. 10, No. 2, Mar. 1996, pp. 123-129. doi: 10.1016/0950-0618(95)00077-1

45. Sæther, I., "Bond Deterioration of Corroded Steel Bars in Concrete," *Structure and Infrastructure Engineering*, V. 7, No. 6, 2011, pp. 415-429. doi: 10.1080/15732470802674836

46. Oh, B. H.; Kim, K. H.; and Jang, B. S., "Critical Corrosion Amount to Cause Cracking of Reinforced Concrete Structures," *ACI Materials Journal*, V. 106, No. 4, July-Aug. 2009, pp. 333-339.

47. Ou, Y.-C.; Fan, H.-D.; and Nguyen, N. D., "Long-Term Seismic Performance of Reinforced Concrete Bridges Under Steel Reinforcement Corrosion due to Chloride Attack," *Earthquake Engineering & Structural Dynamics*, V. 42, No. 14, Nov. 2013, pp. 2113-2127. doi: 10.1002/eqe.2316

48. Cheng, H.; Li, H.-N.; Biondini, F.; Wang, D.-S.; and Zou, Y., "Strain Penetration Effect on Cyclic Response of Corroded RC Columns," *Engineering Structures*, V. 243, Sept. 2021, Article No. 112653. doi: 10.1016/j.engstruct.2021.112653

49. Coronelli, D., and Gambarova, P., "Structural Assessment of Corroded Reinforced Concrete Beams: Modeling Guidelines," *Journal of Structural Engineering*, ASCE, V. 130, No. 8, Aug. 2004, pp. 1214-1224. doi: 10.1061/(ASCE)0733-9445(2004)130:8(1214)

50. Hsu, T. T. C., and Mo, Y.-L., *Unified Theory of Concrete Structures*, John Wiley & Sons, Ltd., Chichester, UK, 2010, 520 pp.

51. Vu, N. S., and Li, B., "Seismic Performance Assessment of Corroded Reinforced Concrete Short Columns," *Journal of Structural Engineering*, ASCE, V. 144, No. 4, Apr. 2018, p. 04018018. doi: 10.1061/(ASCE)ST.1943-541X.0001994

52. Mander, J. B.; Priestley, M. J. N.; and Park, R., "Theoretical Stress-Strain Model for Confined Concrete," *Journal of Structural Engineering*, ASCE, V. 114, No. 8, Sept. 1988, pp. 1804-1826. doi: 10.1061/(ASCE)0733-9445(1988)114:8(1804)

53. Molina, F. J.; Alonso, C.; and Andrade, C., "Cover Cracking as a Function of Rebar Corrosion: Part 2—Numerical Model," *Materials and Structures*, V. 26, No. 9, Nov. 1993, pp. 532-548. doi: 10.1007/BF02472864

54. Tuutti, K., "Corrosion of Steel in Concrete," PhD thesis, KTH Royal Institute of Technology, Stockholm, Sweden, 1982, 474 pp.

55. Stewart, M. G., and Al-Harthy, A., "Pitting Corrosion and Structural Reliability of Corroding RC Structures: Experimental Data and Probabilistic Analysis," *Reliability Engineering & System Safety*, V. 93, No. 3, Mar. 2008, pp. 373-382. doi: 10.1016/j.ress.2006.12.013

56. Nielsen, M.; Braestrup, M.; Jensen, B.; and Bach, F., "Concrete Plasticity-Shear in Beams," *CEB Bulletin D'Information*, No. 126, 1978, pp. 285-357.

57. Thürlimann, B., "Plastic Analysis of Reinforced Concrete Beams," Proceedings of the IABSE Colloquium on Plasticity in Reinforced Concrete, Copenhagen, Denmark, May 1979, pp. 71-90.

58. Bae, S.-W.; Belarbi, A.; and Myers, J. J., "Performance of Corrosion-Damaged RC Columns Repaired by CFRP Sheets," *7th International Symposium on Fiber-Reinforced Polymer (FRP) Reinforcement for Concrete Structures*, SP-230, C. K. Shield, J. P. Busel, S. L. Walkup, and D. D. Gremel, eds., American Concrete Institute, Farmington Hills, MI, 2005, pp. 1447-1464.

59. Revathy, J.; Suguna, K.; and Raghunath, P. N., "Effect of Corrosion Damage on the Ductility Performance of Concrete Columns," *American Journal of Engineering and Applied Sciences*, V. 2, No. 2, 2009, pp. 324-327. doi: 10.3844/ajeassp.2009.324.327

60. Vecchio, F. J., and Collins, M. P., "The Modified Compression-Field Theory for Reinforced Concrete Elements Subjected to Shear," *ACI Journal Proceedings*, V. 83, No. 2, Mar.-Apr. 1986, pp. 219-231.

61. Park, R., "Evaluation of Ductility of Structures and Structural Assemblages from Laboratory Testing," *Bulletin of the New Zealand Society for Earthquake Engineering*, V. 22, No. 3, 1989, pp. 155-166.

62. Li, J.-b., and Gong, J.-x., "Influences of Rebar Corrosion on Seismic Behavior of Circular RC Columns," *China Journal of Highway and Transport*, V. 21, No. 4, July 2008, pp. 55-60. (in Chinese)

63. El Maaddawy, T. A., and Soudki, K. A., "Effectiveness of Impressed Current Technique to Simulate Corrosion of Steel Reinforcement in Concrete," *Journal of Materials in Civil Engineering*, ASCE, V. 15, No. 1, Feb. 2003, pp. 41-47. doi: 10.1061/(ASCE)0899-1561(2003)15:1(41)

64. Xia, J.; Jin, W.-L.; and Li, L.-Y., "Shear Performance of Reinforced Concrete Beams with Corroded Stirrups in Chloride Environment," *Corrosion Science*, V. 53, No. 5, May 2011, pp. 1794-1805. doi: 10.1016/j.corsci.2011.01.058

65. Zhang, R.; Castel, A.; and François, R., "The Corrosion Pattern of Reinforcement and Its Influence on Serviceability of Reinforced Concrete Members in Chloride Environment," *Cement and Concrete Research*, V. 39, No. 11, Nov. 2009, pp. 1077-1086. doi: 10.1016/j.cemconres.2009.07.025

APPENDIX A: NOMENCLATURE LIST

Parameter	Description
$A_{sp,res}$	Mean residual spiral cross-sectional area (mm^2).
b_0	Column circumference (mm).
c	Neutral axis depth (mm).
d	Depth of the confined concrete core (mm).
d'	Depth of the uncracked concrete core (mm).
d_c	Center-to-center diameter of the enclosed spiral (mm).
D	Column diameter (mm).
D'	Corroded dependable column section depth (mm).
$E_{s,res}$	Residual steel elastic modulus (corroded) (GPa).
f_c'	Uncorroded concrete cylinder compressive strength (MPa).
$f_{c,corr}'$	Corroded unconfined concrete compressive strength (MPa).
f_{ccc}	Corroded concrete strength of cracked concrete core portion (MPa).
f_{cc}	Concrete strength of uncracked concrete core (MPa).
f_{yt}	Nominal yield capacity of the transverse reinforcement (MPa).
$f_{yt,res}$	Residual yield capacity of the transverse reinforcement (MPa).
k_e	Confinement effectiveness coefficient.
K	Effective confining pressure (MPa).
L	Column clear height (mm).
i_{corr}	Corrosion current density ($\mu A/cm^2$).
P	Applied axial load (kN).
P_{ave}	Average penetration depth (mm).

$R(i)$	Material loss rate due to corrosion (/year).
R_p	Experimental reduction in peak shear capacity (%).
$R_{\Delta u}$	Experimental reduction in ultimate displacement (%).
s	Spiral spacing (mm).
t	Corrosion duration (days).
V_A	Theoretical nominal shear capacity (assessment) (kN).
V_c	Concrete shear resistance (kN).
V_D	Theoretical nominal shear capacity (design) (kN).
V_p	Shear strength provided by the axial component (kN).
V_s	Steel truss shear mechanism (kN).
w_{cr}	Total surface crack width (mm).
α	Aspect ratio factor.
α_K	Magnification due to confinement.
α_y	Steel yield capacity degradation coefficient.
β	Longitudinal steel ratio factor.
β_E	Steel elastic modulus degradation coefficient.
γ	Displacement ductility factor.
δ	Concrete cover thickness (mm).
Δ_y	Column yield displacement (mm).
Δ_u	Column ultimate displacement (0.85 peak load) (mm).
ε_{cr}	Tensile strain along corrosion cracks (experimental).
$\varepsilon_{cr,t}$	Tensile strain along corrosion cracks (theoretical).
ζ	Concrete softening coefficient.

$\eta_{m,l}$	Average mass loss of the longitudinal reinforcement (%).
$\eta_{m,sp}$	Average mass loss of the transverse spiral reinforcement (%).
θ'	Strut inclination of the corroded column to column axis (degrees).
μ_{Δ}	Displacement ductility capacity.
ν	Web effectiveness factor.
ν_c	Corrosion cracking correction factor.
ν_{cf}	Concrete shear stress (MPa).
ν_{rs}	Volumetric expansion ratio.
ρ_{cc}	Ratio of longitudinal reinforcement to confined core areas.
ρ_l	Longitudinal steel ratio.
$\rho_{sp,res}$	Residual transverse volumetric ratio (corroded).
ϕ	Design strength reduction factor for shear.
ψ	Mechanical degree of shear reinforcement.
ψ_B	Bond failure penalization factor

APPENDIX B: CRACK STATISTICS OF TEST SPECIMENS

Table 1. Crack patterns and key model variables for test specimens included in this study.

Specimen ID	$\sum w_{cr,i} l_i$ (mm^2)	$w_{cr,tot}$ (mm)	ε_{cr} (mm/mm)	ζ_{uc}	f'_c (MPa)	ζ_{cc}	K (MPa)	f_{ccc} (MPa)	f_{cc} (MPa)
BM-UC	0.00	0.00	0.0000	1.00	37.4	1.00	0.858	43.0	43.0
UC-L1	2651	2.47	0.0016	0.65	47.1	0.79	0.565	40.1	50.9
UC-L2 -2.95	4806	3.26	0.0021	0.60	47.1	0.79	0.583	40.3	51.0
UC-M1	3247	3.02	0.0019	0.61	46.7	0.63	0.267	30.5	48.5
UC-M2	2800	2.60	0.0017	0.64	47.1	0.64	0.293	31.3	49.1
UC-S1	2389	2.22	0.0014	0.66	46.7	0.66	0.221	31.9	48.2
UC-S2-2.95	6290	4.26	0.0027	0.56	47.1	0.56	0.333	27.4	49.4
BM-WC	0.00	0.0	0.0000	1.00	35.9	1.00	1.782	47.0	47.0
CS-WC-L1	2313	2.15	0.0014	0.67	56.7	0.79	1.047	50.2	63.7
CS-WC-L2	2455	2.28	0.0015	0.66	46.7	0.79	1.091	42.6	53.9
CS-WC-S1	3504	3.26	0.0021	0.60	56.7	0.60	0.234	35.0	58.3
CS-WC-S2	4310	4.01	0.0026	0.57	56.7	0.57	0.313	33.3	58.9
WD-WC-L1	1482	1.38	0.0009	0.73	56.7	0.79	1.217	51.0	64.7
WD-WC-L2	2221	2.07	0.0013	0.67	38.6	0.79	1.080	36.0	45.6
WD-WC-M1	2866	2.67	0.0017	0.63	56.7	0.63	0.729	39.0	61.6
WD-WC-M2	2814	2.62	0.0017	0.64	47.1	0.64	0.715	33.0	51.9
WD-WC-S1	3256	3.03	0.0019	0.61	56.7	0.61	0.551	37.0	60.4
WD-WC-S2	2642	2.46	0.0016	0.65	46.7	0.65	0.588	32.7	50.7

APPENDIX C: MODEL M-3 SUMMARY

Summarizing all proposed modifications, Eq. 1 – 4 can be amended to account for the effects of material and mechanical degradation on the cyclic shear capacity due to chloride-induced corrosion by taking the structure:

$$V_{A,c} = V_{s,c} + V_{p,c} + V_{c,c} \quad (1)$$

The degraded steel truss mechanism can be expressed as:

$$V_{s,c} = \frac{\pi}{2}\alpha_y(A_{sp,0}f_{yt,0})\frac{D - c' - \delta}{s}\cot(\theta') \quad (2)$$

Where α_y is given in Eq. 10. The adjusted neutral axis c' is derived using the degraded material properties in Eq. 10 and Eq. 16, an equivalent degraded section depth of $D - \delta$ or d for DS2 and DS3 respectively, and the strut inclination θ' is given by the lower-bound approximation in Eq. 30. The degraded axial component is:

$$V_{p,c} = P\frac{(D' - c')}{2L}, \qquad for\ N > 0 \quad (3)$$

Where D' is the dependable depth of the deteriorated section to support axial load, given by Eq. 32.

$$V_{c,c} = \alpha\beta\nu_c\psi_B\gamma_c\sqrt{f_c'} \cdot 0.8(\sqrt{\zeta_{uc}}A_{cover} + \sqrt{\zeta_{cc}\alpha_K}A_{crackedcore} + \sqrt{\alpha_K}A_{core}) \quad (4)$$

The α and β factors remain unchanged and are taken from Eq. 5 and 6. The displacement ductility factor, γ_c, is derived by first developing the degraded shear envelope using Eq. 33 to 39. γ_c is determined by the shear envelope's intercept with the column's force-displacement response. The softening coefficients, ζ_{uc} and ζ_{cc}, are given by Eq. 18, using either Eq. 20 or 23, respectively. The section areas A_{cover}, $A_{crackedcore}$, and A_{core} are derived from Fig. 3.